Eur. Phys. J. Plus (2023) 138:340
https://doi.org/10.1140/epjp/s13360-023-03909-2

THE EUROPEAN PHYSICAL JOURNAL PLUS

Regular Article

The computation of the average speckle size from the point spread function for triangular apertures

A. M. Hamed[a]

Physics Department, Faculty of Science, Ain Shams University, Cairo 11566, Egypt

Received: 19 December 2022 / Accepted: 17 March 2023

Abstract We suggest triangular aperture modeling for the computation of speckle size using the point spread function (PSF) concept. The fast Fourier transform (FFT) algorithm indicates three models of triangular apertures in the point spread function (PSF) computation. We calculated for the first time the average speckle size from the full width at half maximum (FWHM) for the triangular apertures in the PSF. The results are compared with the speckle sizes results obtained from the autocorrelation of speckle images corresponding to the considered models showed an agreement. In the analysis, I consider the 1st model with four equilateral triangular apertures, each of equal sides (b), along the Cartesian coordinates at equal distances from the center (x_d). In the 2nd model, I assume 16 triangular apertures in a circular contour. In contrast, in the 3rd model, a sequence of six equilateral triangular black and white (B/W) zones is shown where the central triangle is black. I consider central obstruction to attenuate the low spatial frequency in the PSF. I take a transparent triangular aperture for comparison. Also, the PSF corresponding to the circular aperture is given for comparison. In addition, reconstructed images of apertures from the speckle images are obtained. We considered MATLAB codes for all the computations and plots.

1 Introduction

The proposal of suggesting a triangular aperture is due to the following reasons. To my knowledge, this aperture is a type of aperture not considered before in microscopic imaging. Since the microscopic resolution is dependent on the aperture and the wavelength of the illumination, we computed the point spread function (PSF) corresponding to these triangular shapes of modulated aperture. In addition, we apply these new triangular apertures in the formation of speckle images using a random diffuser. Consequently, we get the average speckle size using the full width at half maximum (FWHM) obtained from the PSF and compare it with the autocorrelation of speckle images.

The speckle size is produced from the convolution of the PSF corresponding to the aperture and the Fourier spectrum of the diffuser. Hence, the speckle pattern is produced from this convolution. Consequently, we get the average speckle size from the FWHM of the PSF obtained for the aperture. It is assumed monochromatic light for illumination.

The aperture filtering suggested an annular shape for the resolution improvement realized by many authors like in [1–9].

Hamed and Clair [10, 11] proposed and investigated linear and quadratic apertures filtering methods. Recently, we studied a linear-quadratic arrangement in [12]. Recently, we explored a rectangular cranny and the application provided in speckle imaging [13].

The estimation of speckle size by using the FWHW with other modulated apertures was explored by the author [14, 15]. In [14], the contrast of laser speckle images using some modulated apertures was investigated, while in [15], the speckle size was computed by using a Hermite–Gaussian laser beam.

In other fields uses also FWHM for speckle size, for instance in medical applications, the resolving of the lateral component of blood flow velocity based on ultrasound speckle size change with scan direction and speed was given in [16], and ultrasound speckle size and lesion signal-to-noise ratio computed in [17].

In this paper, we present a new triangular arrangement of apertures and compute the PSF and the autocorrelation corresponding to these apertures. In addition, I give an application on speckle imaging modulated by the gap getting reconstructed images. The motivation to get the results is due to the truncation of the legs in the PSF compared with the legs that appeared in the PSF for circular aperture as shown in Fig. 4d, e. A conclusion follows theoretical analysis, results, and discussion.

[a] e-mail: amhamed73@hotmail.com (corresponding author)

Published online: 18 April 2023

2 Methods

2.1 Theoretical analysis

We consider the first model four equilateral triangular apertures, each of equal sides (b), along the Cartesian coordinates at equal distances from the center (x_d) as shown in Fig. 1a. The whole matrix has dimensions of 1024×1024 pixels. A uniform illumination emitted from a laser beam is incident upon this new aperture; hence, the amplitude transmittance is written as follows:

$$A(x, y) = \text{tri}(x - x_d, y) + \text{tri}(x + x_d, y) + \text{tri}(x, y - y_d) + \text{tri}(x, y + y_d) \tag{1}$$

Using the properties of convolution, we substitute the shifted triangular gaps with a triangle at the center convoluted with the shifted Dirac-delta function. Hence, rewrite Eq. (1) as follows:

$$\begin{aligned} A(x, y) = {} & \text{tri}(x, y) \otimes \delta(x - x_d, y) + \text{tri}(x, y) \otimes \delta(x + x_d, y) \\ & + \text{tri}(x, y) \otimes \delta(x, y - y_d) + \text{tri}(x, y) \otimes \delta(x, y + y_d) \end{aligned} \tag{2}$$

At the same time, with the convolution properties, we write the triangular aperture equal to the autocorrelation of the rectangular aperture of width $a = b/2$ as follows:

$$\text{tri}(x, y) = \text{rect}(x, y) \otimes \text{rect}(x, y) \tag{3}$$

We consider the triangular width b to be equal to two times the rectangular aperture.

Substituting Eq. (3) in Eq. (2), we get:

$$A(x, y) = \text{rect}(x, y) \otimes \text{rect}(x, y) \otimes \{\delta(x - x_d, y) + \delta(x + x_d, y) + \delta(x, y - y_d) + \delta(x, y + y_d)\} \tag{4}$$

We obtained the point spread function (PSF) corresponding to the novel aperture described by Eq. (4) by operating the Fourier transform as follows:

$$\begin{aligned} h(x, y) &= \text{F.T.}[A(x, y)] \\ &= \text{F.T.}[\{\text{rect}(x, y) \otimes \text{rect}(x, y)\} \otimes \{\delta(x - x_d, y) + \delta(x + x_d, y) + \delta(x, y - y_d) + \delta(x, y + y_d)\}] \end{aligned} \tag{5}$$

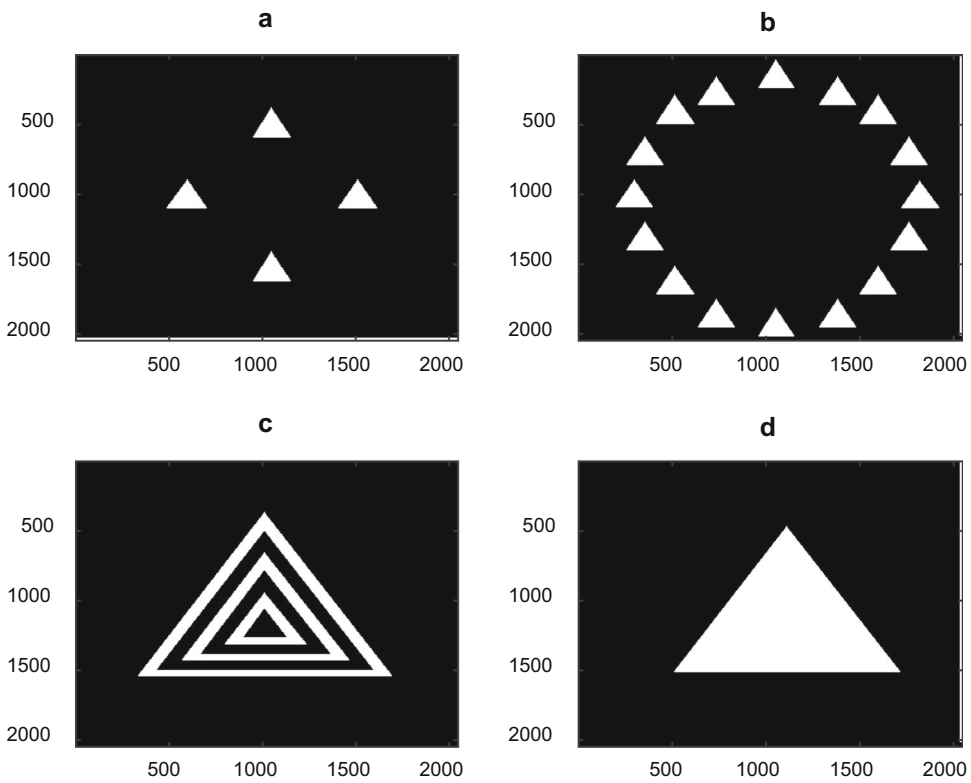

Fig. 1 a–d The gap of four triangles arranged symmetrically along the Cartesian coordinates in (**a**). In **b**, I plot 16 equilateral triangles in a contour with a radius of nearly = 900 pixels. In **c**, I showed six concentric B/W triangles where the external triangle length = 1349 pixels. In **d**, I give a transparent equilateral triangle of side length = 1192 pixels

We write the known Fourier transform of autocorrelation of rectangular function as the simple product of the F.T. corresponding to each rectangular part:

$$\text{F.T.}\{\text{rect}(x, y) \otimes \text{rect}(x, y)\} = \text{F.T.}\{\text{rect}(x, y)\} \cdot \text{F.T.}\{\text{rect}(x, y)\} \tag{6}$$

Hence, we get the following result for the F.T. of the triangular function:

$$\begin{aligned}\text{F.T.}\{\text{tri}(x, y)\} &= \text{F.T.}\{\text{rect}(x, y) \otimes \text{rect}(x, y)\} \\ &= a^4 \left[\frac{\sin\left(\frac{\pi a u}{\lambda f}\right)}{\left(\frac{\pi a u}{\lambda f}\right)}\right]^2 \left[\frac{\sin\left(\frac{\pi a v}{\lambda f}\right)}{\left(\frac{\pi a v}{\lambda f}\right)}\right]^2 \\ &= a^4 \sin c^2\left(x'\right) \sin c^2\left(y'\right)\end{aligned} \tag{7}$$

where we define the $\sin c$ function as follows:

$\sin c\left(x'\right) = \frac{\sin(\pi x')}{\pi x'}$, $x' = \frac{au}{\lambda f}$, $b = 2a$. And we get a similar expression for $\sin c\left(y'\right)$.

We rewrite Eq. (7), substituting the triangle width $b = 2a$ as follows:

$$\text{F.T.}\{\text{tri}(x, y)\} = (b^4/16)\left[\frac{\sin\left(\frac{\pi b u}{2\lambda f}\right)}{\left(\frac{\pi b u}{2\lambda f}\right)}\right]^2 \left[\frac{\sin\left(\frac{\pi b v}{2\lambda f}\right)}{\left(\frac{\pi b v}{2\lambda f}\right)}\right] \tag{8}$$

The Fourier transform of shifted Dirac-delta function gives an inclined plane wave as:

$$\begin{aligned}\text{F.T.}\{\delta(x - x_d, y)\} &= \int\int_{-\infty}^{\infty} \delta(x - x_d, y) \exp\left[-\frac{j2\pi}{\lambda f}(xu + yv)\right] \mathrm{d}x\, \mathrm{d}y \\ &= \exp\left(-\frac{j2\pi x_d u}{\lambda f}\right) \int\int_{-\infty}^{\infty} \delta(x - x_d, y) \\ &\quad \times \exp\left[-\frac{j2\pi}{\lambda f}((x - x_d)u + yv)\right] \mathrm{d}x\, \mathrm{d}y \\ &= \exp\left(-\frac{j2\pi x_d u}{\lambda f}\right)\end{aligned} \tag{9}$$

We obtained similar expressions for the other shift of the Dirac-delta function in Eq. (5) as follows:

Plugging Eqs. (8, 9) in Eq. (5), we get:

$$\begin{aligned}h(x, y) = \frac{b^4}{16} &\left[\frac{\sin\left(\frac{\pi b u}{2\lambda f}\right)}{\left(\frac{\pi b u}{2\lambda f}\right)}\right]^2 \left[\frac{\sin\left(\frac{\pi b v}{2\lambda f}\right)}{\left(\frac{\pi b v}{2\lambda f}\right)}\right]^2 \\ &\times \left\{\exp\left(-\frac{j2\pi x_d u}{\lambda f}\right) + \exp\left(+\frac{j2\pi x_d u}{\lambda f}\right)\right. \\ &\left. + \exp\left(-\frac{j2\pi y_d v}{\lambda f}\right) + \exp\left(+\frac{j2\pi y_d v}{\lambda f}\right)\right\}\end{aligned} \tag{10}$$

Hence, we finally write the PSF as follows:

$$\begin{aligned}h(x, y) = \frac{b^4}{8} &\left[\frac{\sin\left(\frac{\pi b u}{2\lambda f}\right)}{\left(\frac{\pi b u}{2\lambda f}\right)}\right]^2 \left[\frac{\sin\left(\frac{\pi b v}{2\lambda f}\right)}{\left(\frac{\pi b v}{2\lambda f}\right)}\right]^2 \\ &\times \left\{\cos\left(\frac{2\pi x_d u}{\lambda f}\right) + \cos\left(\frac{2\pi y_d v}{\lambda f}\right)\right\}\end{aligned} \tag{11}$$

We rewrite Eq. (11) as follows:

$$\begin{aligned}h(x, y) = \frac{b^4}{4} &\left[\frac{\sin\left(\frac{\pi b u}{2\lambda f}\right)}{\left(\frac{\pi b u}{2\lambda f}\right)}\right]^2 \left[\frac{\sin\left(\frac{\pi b v}{2\lambda f}\right)}{\left(\frac{\pi b v}{2\lambda f}\right)}\right]^2 \\ &\times \left\{\cos\left(\frac{\pi(x_d u + y_d v)}{\lambda f}\right) \cos\left(\frac{\pi(x_d u - y_d v)}{\lambda f}\right)\right\}\end{aligned} \tag{12}$$

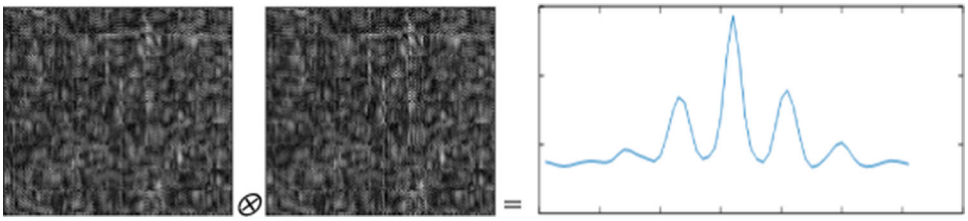

Fig. 2 The autocorrelation plot corresponding to the modulated speckle intensity

The intensity impulse response is computed from the modulus square of Eq. (12) as follows:

$$I(x,y) = \frac{b^8}{16}\left[\frac{\sin\left(\frac{\pi bu}{2\lambda f}\right)}{\left(\frac{\pi bu}{2\lambda f}\right)}\right]^4\left[\frac{\sin\left(\frac{\pi bv}{2\lambda f}\right)}{\left(\frac{\pi bv}{2\lambda f}\right)}\right]^4 \times\left\{\cos^2\left(\frac{\pi(x_d u + y_d v)}{\lambda f}\right)\cos^2\left(\frac{\pi(x_d u - y_d v)}{\lambda f}\right)\right\} \tag{13}$$

2.2 Computation of the speckle size from the PSF corresponding to the apertures

We apply the FFT to the triangular models and we get the PSF or amplitude impulse response. We compute the FWHM from the PSF curves and we get the average speckle size. We get the modulated speckle as the convolution of the PSF corresponding to the apertures and the Fourier spectrum of the diffuser as outlined by Eq. (16) in the next Sect. 2.3.

2.3 Computation of the speckle size from the autocorrelation of speckle images

We construct modulated speckle images using collimated laser beam incident upon the triangular aperture $A(x, y)$ Eq. (1) followed by a diffuser $d(x, y)$. In the focal plane of a converging lens, we get the FT of the multiplication of the aperture and the diffuser which represents the modulated speckle images. We summarize the process as follows:

$$B(x,y) = A(x,y)\cdot d(x,y) \tag{14}$$

where the diffuser is represented by a randomly distributed function as in [14]:

$$d(x,y) = a(x,y)\exp\{2\pi i\cdot \mathrm{rand}(x,y)\}; i = \sqrt{-1} \tag{15}$$

$a(x, y)$ its amplitude and $\exp\{2\pi i \cdot \mathrm{rand}(x, y)\}$ its phase with random variation.

$$\begin{aligned} B(u,v) = FT\{B(x,y\} &= FT\{A(x,y)\cdot d(x,y)\} = FT\{A(x,y\}\otimes FT\{d(x,y\} \\ &= A(u,v)\otimes d(u,v) \end{aligned} \tag{16}$$

$\otimes$ is a symbol for convolution operation. We write the complex amplitude Eq. (16) in integral form as follows:

$$B(u,v) = \int_{-\infty}^{\infty}\int A(u-u', v-v')d(u',v')du'dv' \tag{17}$$

We get the modulated speckle intensity as the modulus square of Eq. (16). Hence, we computed the average speckle size from the full width at half maximum (FWHM) corresponding to the autocorrelation plot using the graph shown in Fig. 2. The details of the autocorrelation plot are shown in Fig. 12a, b. We rewrite the autocorrelation symbolically as follows:

$$C(u,v) = I(u,v)\otimes I(u,v); \tag{18}$$

Reference [14].

3 Results

Using MATLAB code, we showed the newly equilateral triangular apertures in Fig. 1a. We consider the gap of four triangles arranged symmetrically along the Cartesian coordinates in the analysis Fig. 1a. We have the four triangles at the coordinates where the approximate triangle length is equal to 210 pixels in a matrix of dimensions 1024×1024 pixels. In Fig. 1b, we plot 16 equilateral triangles in a contour of a radius of nearly 900 pixels. In Fig. 1c, we showed six concentric B/W triangles where the external triangle length (1701–352) equals 1349 pixels. Its coordinates are the following {(1024, 346), [(352, 1546), (1071, 1555)]}. In Fig. 1d, we give a transparent equilateral triangle of side length (1724–532) equal to 1192 pixels.

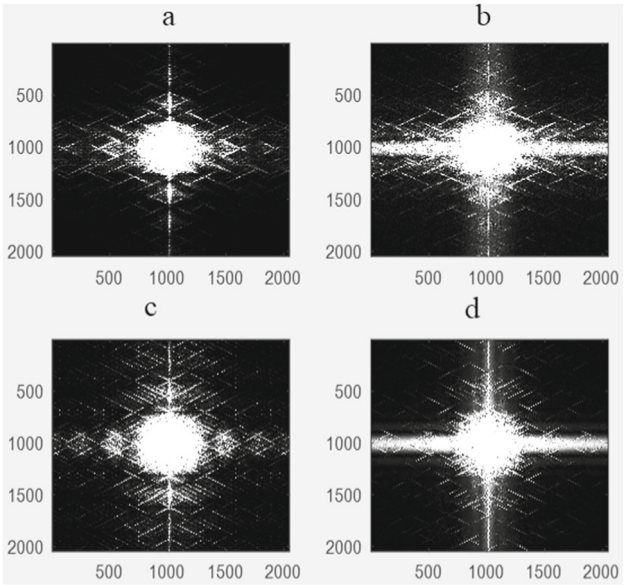

Fig. 3 **a–d** The PSF images are shown in (**a–d**) corresponding to the apertures described in the statistics (**a–d**)

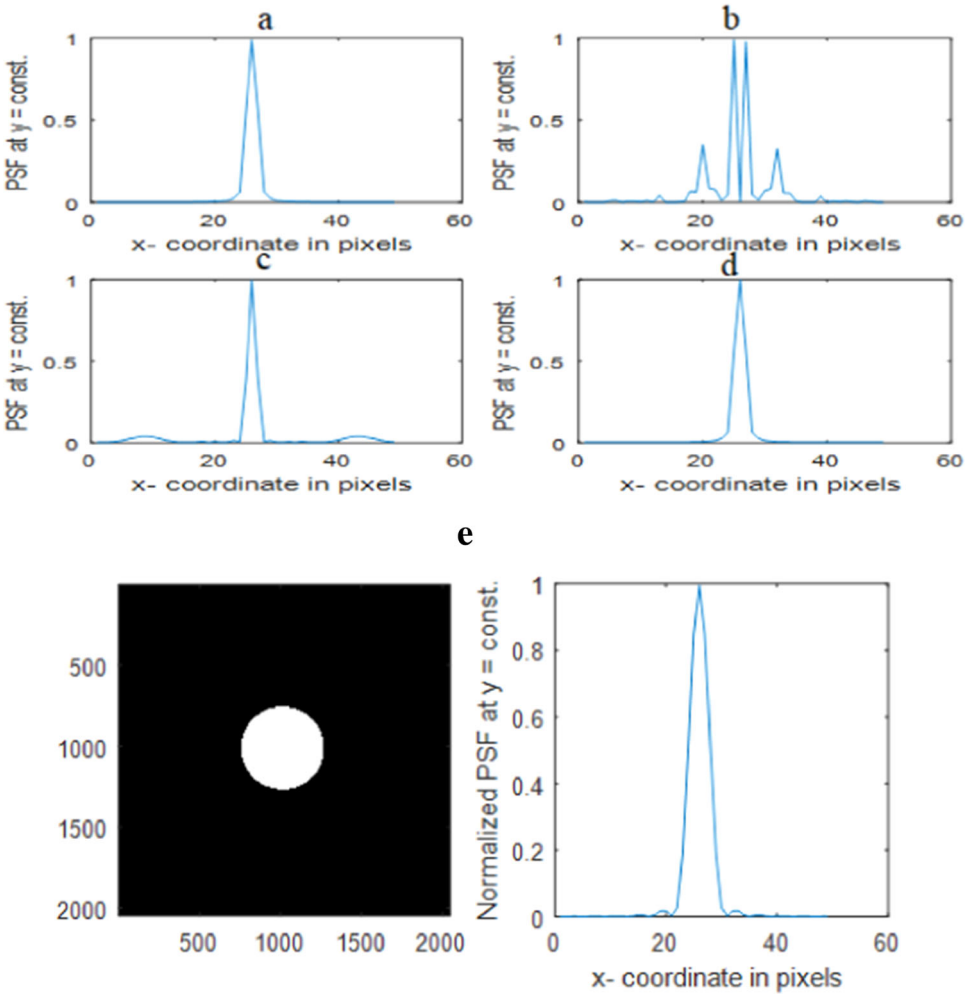

Fig. 4 **a–d** The PSF plots corresponding to the apertures in (**a–d**) at constant altitude y equal to 1024 pixels. **e** The PSF plots corresponding to the circular aperture at constant altitude y equal to 1024 pixels. It is shown that the secondary legs of the diffraction pattern are dominant compared with the triangular aperture in (**d**). The FWHM is the same as the triangular aperture where the radius = 256 pixels in both apertures

We computed the PSF corresponding to the apertures under investigation using the FFT technique. We represent the intensity impulse response or the modulus square of the PSF in Fig. 3a–d corresponding to the apertures described in the statistics (Fig. 1a–d).

Table 1 Computation of the average speckle size from the FWHM using both PSF plots and the autocorrelation of speckle images

Aperture shape	FWHM from PSF in pixels	FWHM from the autocorrelation of speckles in pixels
1. Four triangles along the Cartesian coordinates	5	5
2. Sixteen triangles along a circular contour	3	3
3. B/W Concentric triangles	4	5
4. Transparent triangle	5	6

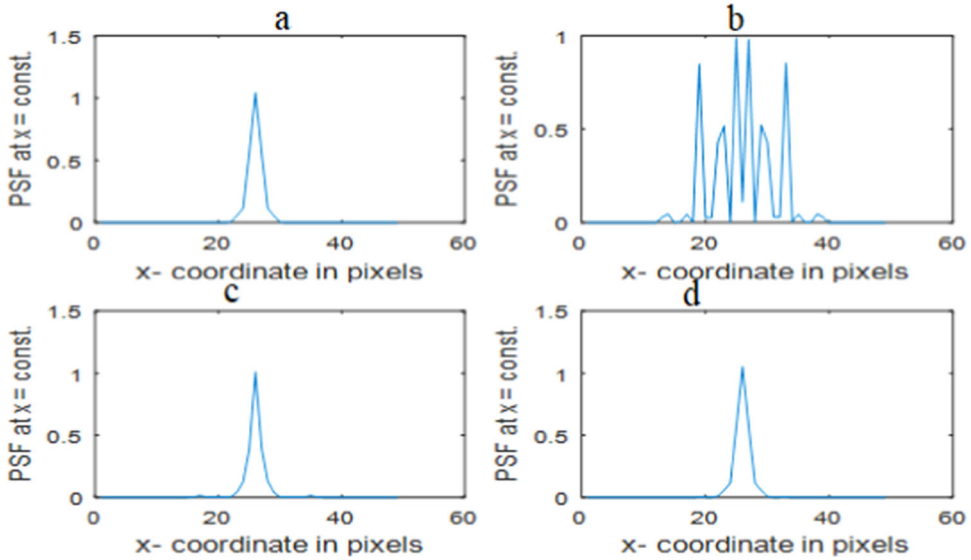

Fig. 5 a–d The PSF plots corresponding to the apertures in (**a–d**) at constant altitude x equal to 1024 pixels

We plot the PSF from 1000 to 1048 pixels at constant altitude y equal to 1024 pixels shown in Fig. 3a–d corresponding to the images in Fig. 3a–d, respectively. We computed the FWHM corresponding to the plots in Fig. 4a–d, and we get the following results represented in Table 1. In contrast, we compared it with the autocorrelation FWHM plotted in the same table as shown in Figs. 12, 13, and 14 discussed later. We considered the FWHM to represent the average speckle size.

In contrast, we plot the PSF from 1000 to 1048 pixels at constant altitude x equal to 1024 pixels shown in Fig. 5a–d corresponding to the images in Fig. 3a–d, respectively.

We showed the autocorrelation images of the apertures shown in Fig. 6a–d. In contrast, we showed the plots corresponding to the autocorrelation images as in Fig. 7a–d. We computed the autocorrelation images using the FFT algorithm where the range of the autocorrelation is from 1 to 1024 pixels.

We showed the speckle images and the reconstructed images corresponding to all the triangular models in Fig. 8a–d. We computed the speckle images using the FFT algorithm operated on the diffuser followed by the triangular models. In contrast, we get the reconstructed images by operating the FFT upon the complex amplitudes corresponding to the speckle images.

The speckle images corresponding to the four triangular apertures at different altitudes at y equal to 90, 128, and 200 pixels are shown in Fig. 9a and at altitudes at y equal to 110, 150, and 220 pixels as in Fig. 9b. We give the magnified zones of the plots in the range from 200 to 256 pixels at y equal to 110, 150, and 220 pixels as in Fig. 10.

We showed in Fig. 11, the Speckle image of 256×256 pixels modulated by four triangular apertures (a), and the corresponding autocorrelation plot in (b) in the range from 226 to 286 pixels. We computed the FWHM, as shown in Fig. 11, as equal to five pixels. In Fig. 12, we showed the speckle image and its autocorrelation for 16 triangular apertures, and we computed the FWHM as equal to three pixels. In contrast, we get in Fig. 13, the FWHM shown in Fig. 13 is equal to five pixels where we considered concentric B/W triangles of the center dark. We compared the above results of correlation with that obtained in the transparent triangle and we get the FWHM is equal to six pixels as in Fig. 14.

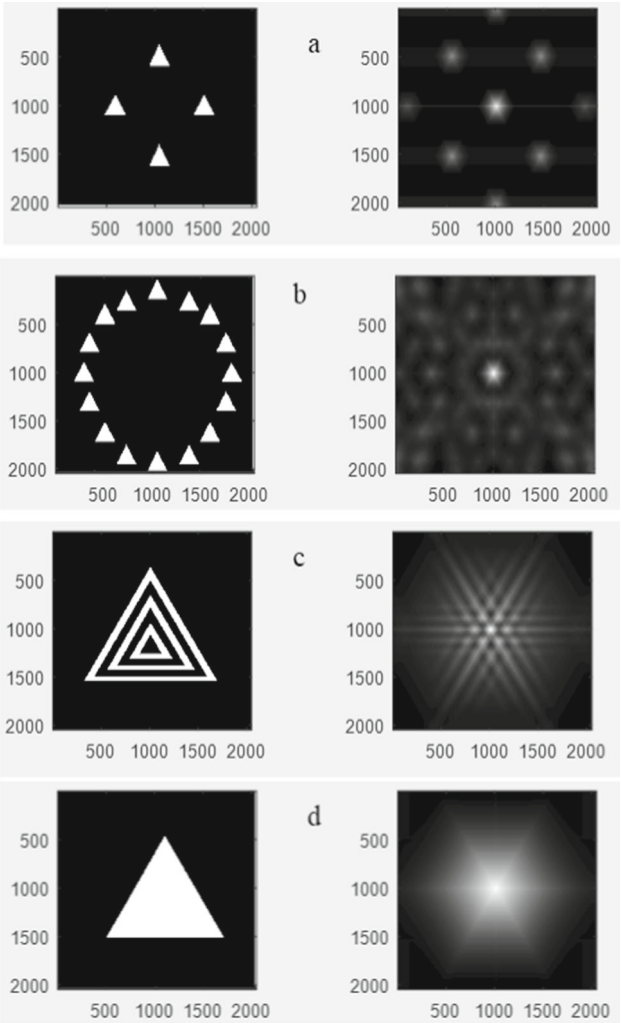

Fig. 6 a–d The triangular models are shown in the L.H.S., and the corresponding autocorrelation images are shown in the R.H.S

4 Discussion

The intensity impulse response or the modulus square of the PSF we computed for the triangular models in Fig. 1a–d showed little difference except for the B/W concentric annuli in Fig. 3c. The intensity in Fig. 2c showed the diffraction pattern of detachable legs compared with the other models in Fig. 3a, b, d. Hence, we established a difference in the plots as in the statistics (Fig. 4a–d) at constant y. We have similar PSF plots corresponding to the four triangular actions along the Cartesian coordinates and the single triangular aperture as in Fig. 4a, d. In contrast, we have a distinguished pattern for the PSF for the 16 triangles along the circular contour. It has two symmetrical spikes around the center, and we observed faint legs around the center as in Fig. 4b. In this case, we believe the PSF is useful for extended imaging objects. At the same time, we have PSF with a bright central lobe surrounded by detachable legs as in Fig. 4c, corresponding to the model of B/W concentric triangles.

The PSF plot corresponding to the circular aperture at constant altitude y equal to 1024 pixels is given for comparison as in Fig. 4e. It is shown that the secondary legs of the diffraction pattern are dominant compared with the triangular aperture in Fig. 4d. The FWHM is the same as the triangular aperture where the radius = 256 pixels in both cases.

We established a similarity in the PSF plots as in the statistics (Fig. 5a–d) at constant x except for that corresponding to the 16 triangles around a circular contour with six peaks around the center and the other two faint peaks as in Fig. 5b. Hence, it confirms the PSF is useful for extended imaging objects.

We were referring to the autocorrelation images in Fig. 6. In the 1st model of four rectangles, we showed nine bright spots, four along the Cartesian coordinates, and another four areas along the diagonal. In addition, we observed the central luminous area as in Fig. 6a. In contrast, in the model of 16 equilateral triangles in a nearly circular contour, we observed a prominent bright spot surrounded by a hexagonal shape and many patches almost two times the number of rectangles as in Fig. 6b. While in the 3rd model, of six concentric B/W triangles, we showed many patches around the center with lines parallel to the triangle sides as in Fig. 6c. We

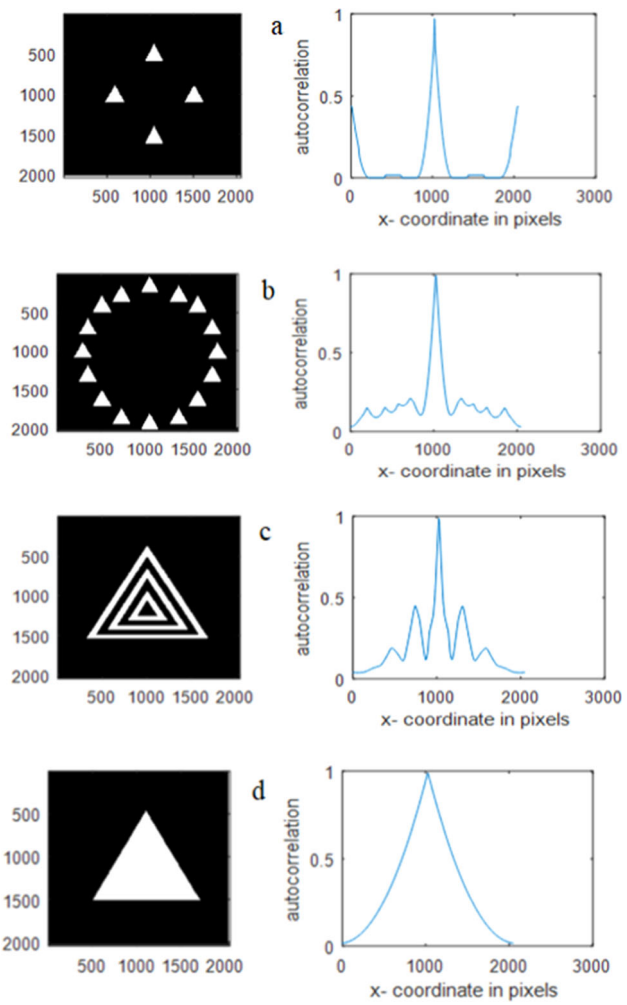

Fig. 7 a–d The triangular models are shown in the L.H.S., and the corresponding autocorrelation plots are shown in the R.H.S

compared the above autocorrelation images with the standard autocorrelation corresponding to the triangular aperture. It has only a hexagonal shape of a central bright spot as in Fig. 6d.

We showed line plots along the direction x corresponding to the autocorrelation images in Fig. 6 and plotted as in Fig. 7a–d. In the 1st model, with four triangular apertures along the coordinates, we showed a central peak beside two side peaks (Fig. 7a), as expected from the corresponding autocorrelation image. In contrast, in the 2nd model, with 16 triangles along a circular contour, we observed eight side peaks surrounding the central peak as in Fig. 7b. Hence, we showed two side peaks in the 1st model compared to eight in the 2nd model. Consequently, the 2nd model of 16 triangles has four autocorrelation side peaks corresponding to the 1st model.

While in the 3rd model of six B/W concentric triangles, we observed only four side peaks surrounding the central peak Fig. 7c compared with the standard decaying distribution corresponding to the transparent triangular aperture.

In Fig. 7d, we also showed that in the transparent triangular aperture, the total bandwidth is equal to 2048 pixels, twice the aperture width of 1188 pixels, with an error = 16% deviated from the ideal value of 1024 pixels.

We showed referring to Fig. 8a–d that the reconstructed images from the speckle images are affected by the diffuser noise. In addition, all speckle images are different and depend on the aperture shape. In the speckle plots in the range from 200 to 256 pixels at constant altitude y equal to 128 pixels, we showed different profiles indicating their dependence on the triangular shapes as in Fig. 9a, b. The same plots we showed were different in Fig. 10 in the whole range from one to 256 pixels.

We showed, referring to Figs. 12, 13, and 14, that different values of FWHM ranging from three to six pixels represent the speckle sizes corresponding to the different aperture geometries shown in Table 1.

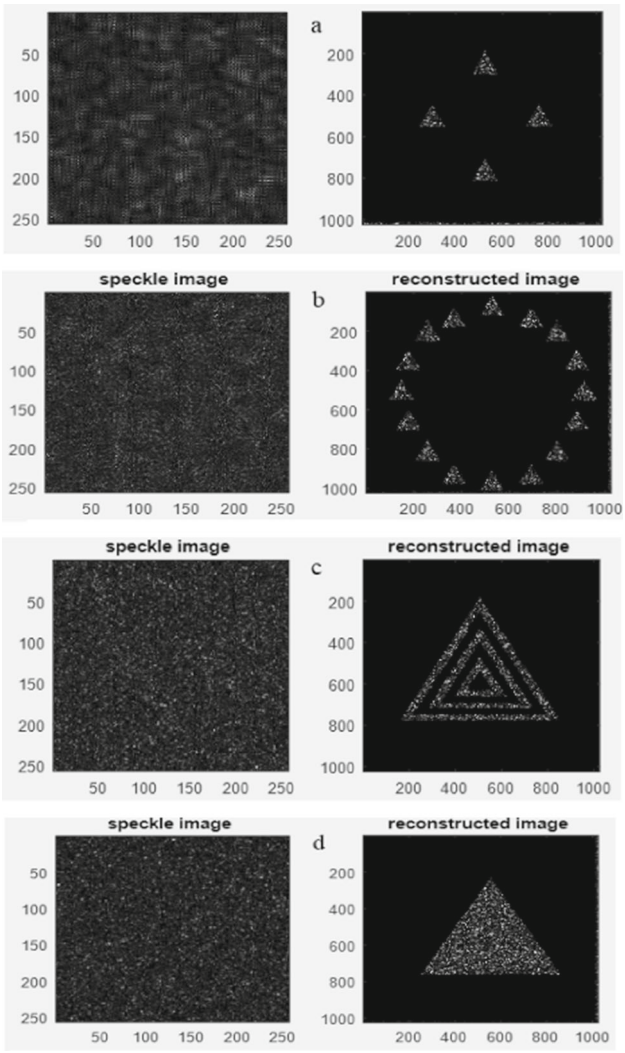

Fig. 8 a–d The modulated speckle images are shown in the L.H.S., and the corresponding reconstructed images are in the R.H.S

5 Conclusions

We concluded that referring to the PSF plots (Figs. 4b and 5b), the 16 triangular aperture is helpful for extended imaging of objects. We got several peaks around the center compared with the pure triangular aperture. We differentiate the models of triangular apertures referring to the different autocorrelation images as shown in Fig. 6.

We conclude from the plots in Fig. 7 that the 2nd model of 16 triangles has four autocorrelation side peaks corresponding to the 1st model. In contrast, we showed only four autocorrelation side peaks surrounding the central peak in the 3rd model of the B/W concentric triangular aperture of six zones. We get different autocorrelation side peaks in all the models compared with the corresponding transparent triangle of decaying intensity from the center. Consequently, the autocorrelation corresponding to the different shapes of triangular apertures showed a geometry related to its distribution.

We showed the irregularities in the speckle pattern dependent on the geometry of the aperture for the same diffuser as shown in Figs. 9 and 10. This is attributed to the convolution of the aperture PSF and the diffuser spectrum.

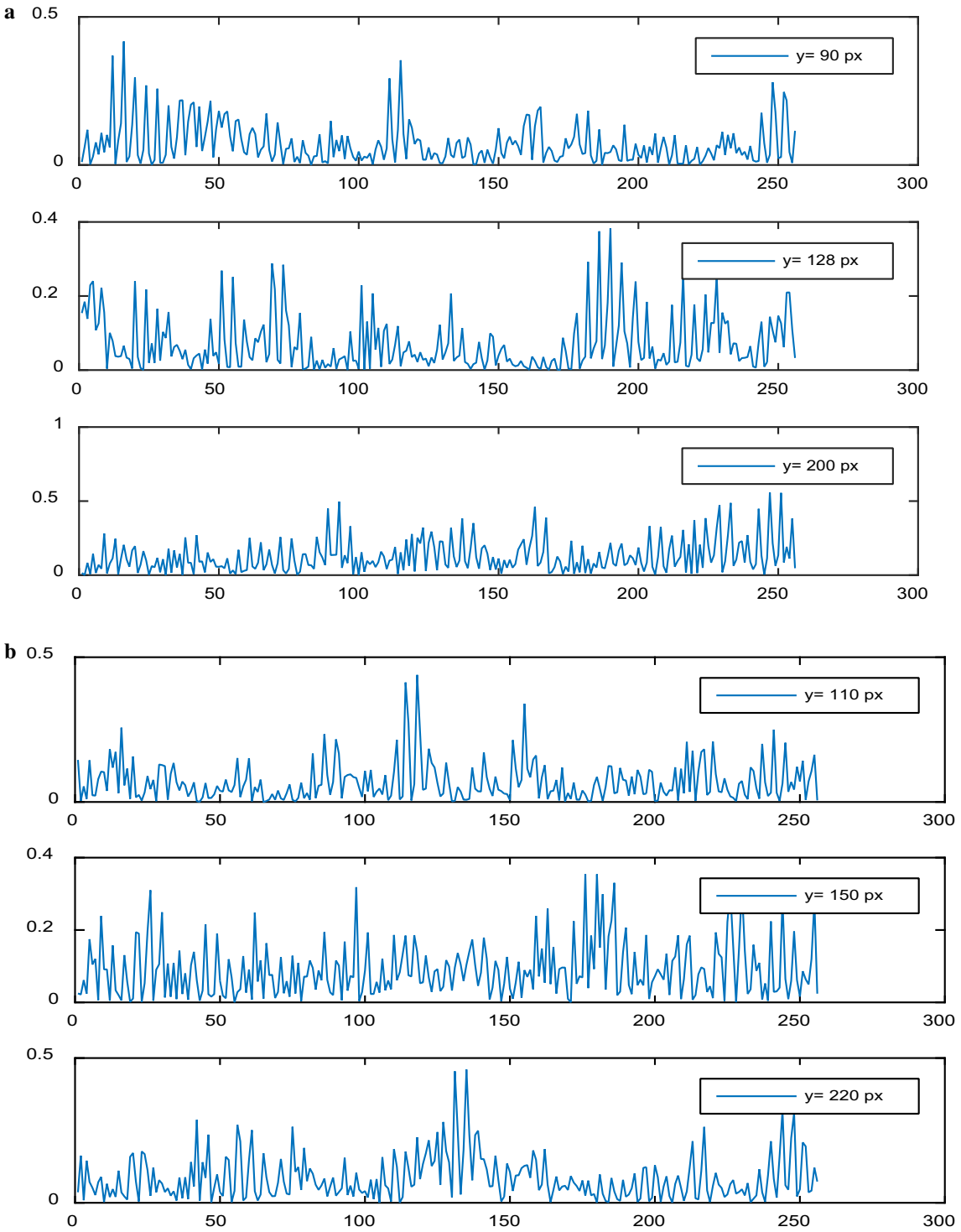

Fig. 9 **a** Speckle plot corresponding to four triangular apertures (model 1) at *y* equal to 90, 128, and 200 pixels. **b** Speckle plot corresponding to four triangular apertures (model 1) at *y* equal to 110, 150, and 220 pixels

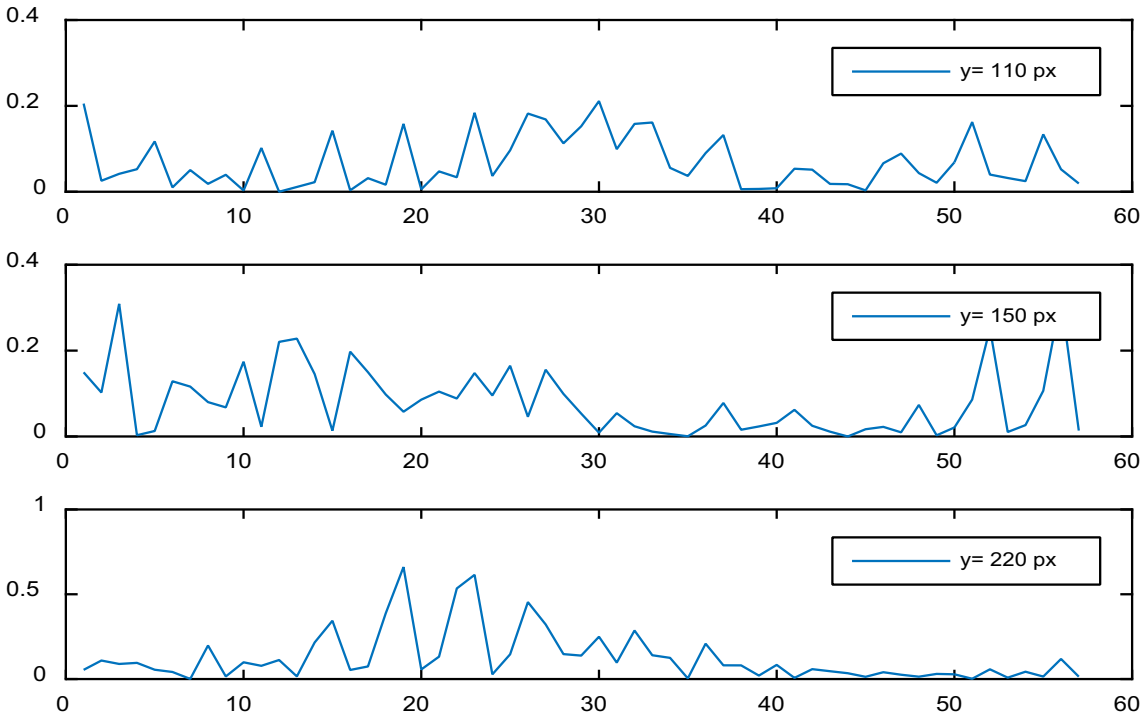

Fig. 10 speckle plot at *y* equal to 110, 150, and 220 pixels in the range from 200 to 256 pixels

Fig. 11 **a, b** Speckle image of 256×256 pixels modulated by four triangular apertures (**a**), and the corresponding autocorrelation plot in (**b**) in the range from 226 to 286 pixels. The FWHM is computed as shown in the legend equal to five pixels

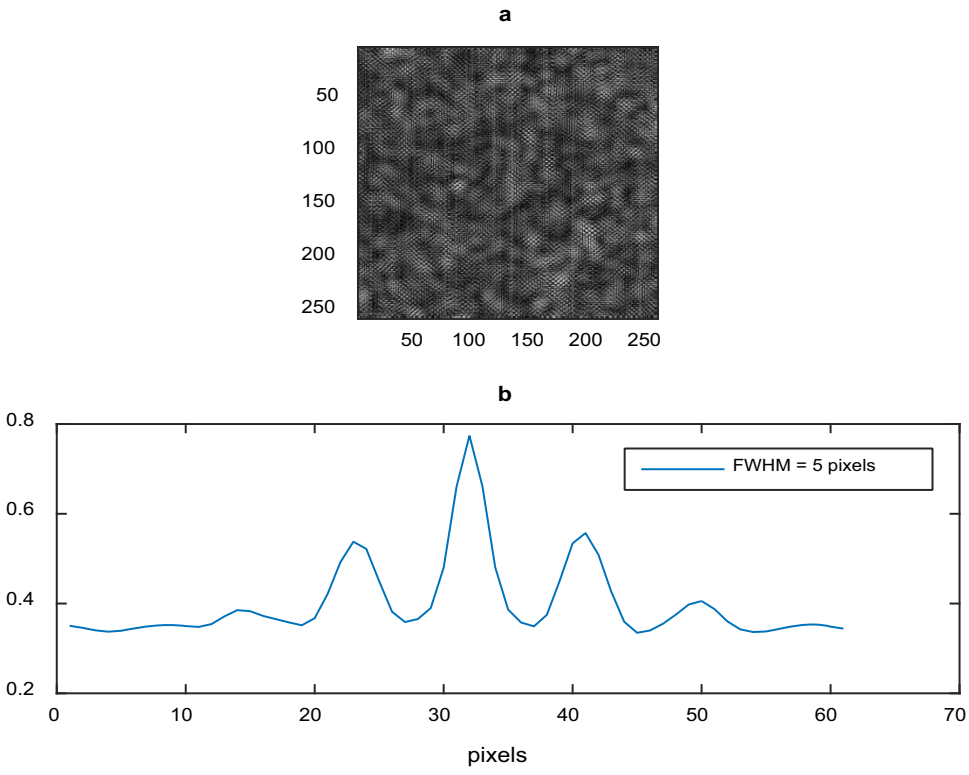

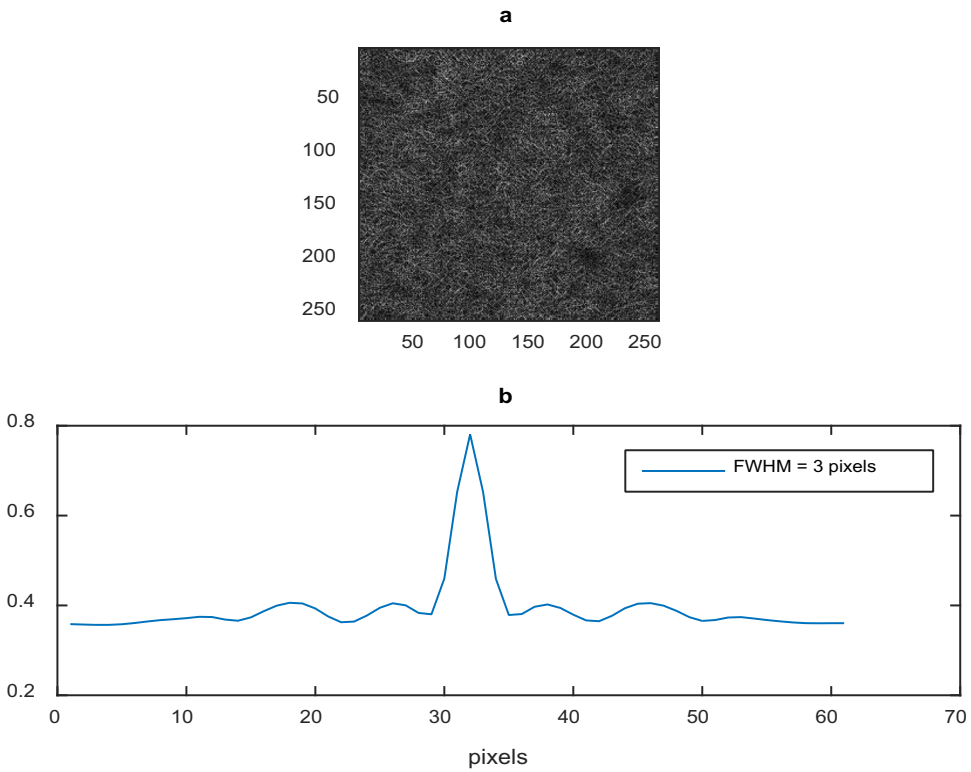

Fig. 12 **a, b** Speckle image modulated by 16 triangular apertures (**a**), and the corresponding autocorrelation plot in (**b**) in the range from 226 to 286 pixels. The FWHM is computed as shown in the legend equal to three pixels

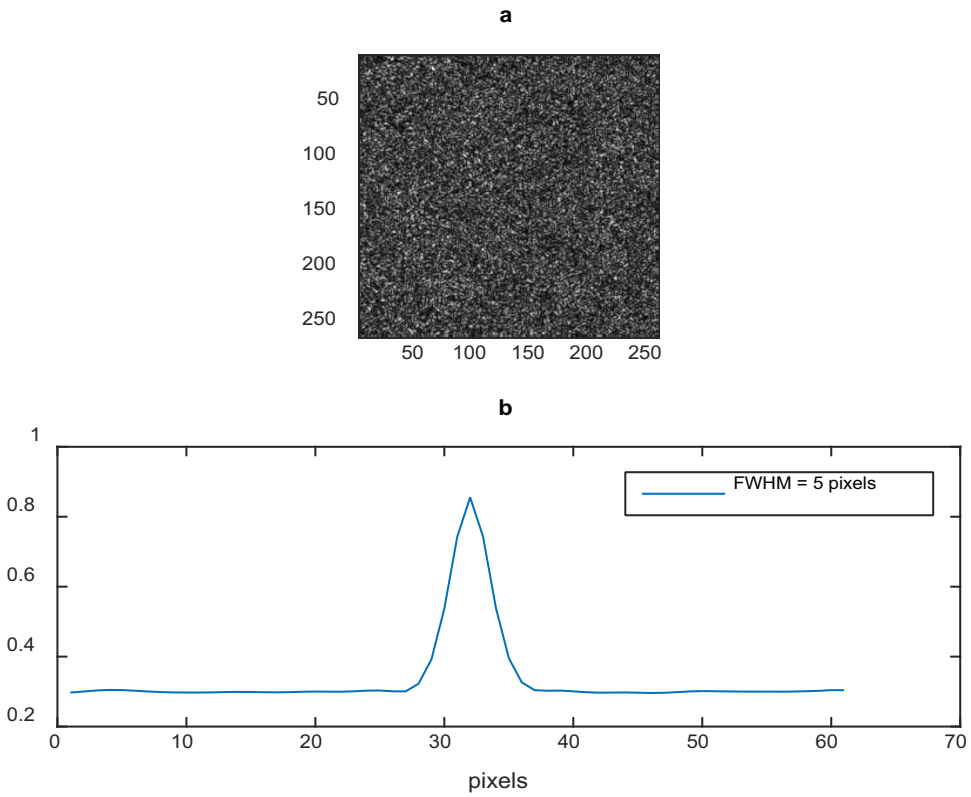

Fig. 13 **a, b** Speckle image modulated by concentric B/W triangular aperture (**a**), and the corresponding autocorrelation plot in (**b**) in the range from 226 to 286 pixels. The FWHM is computed as shown in the legend equal to 5 pixels

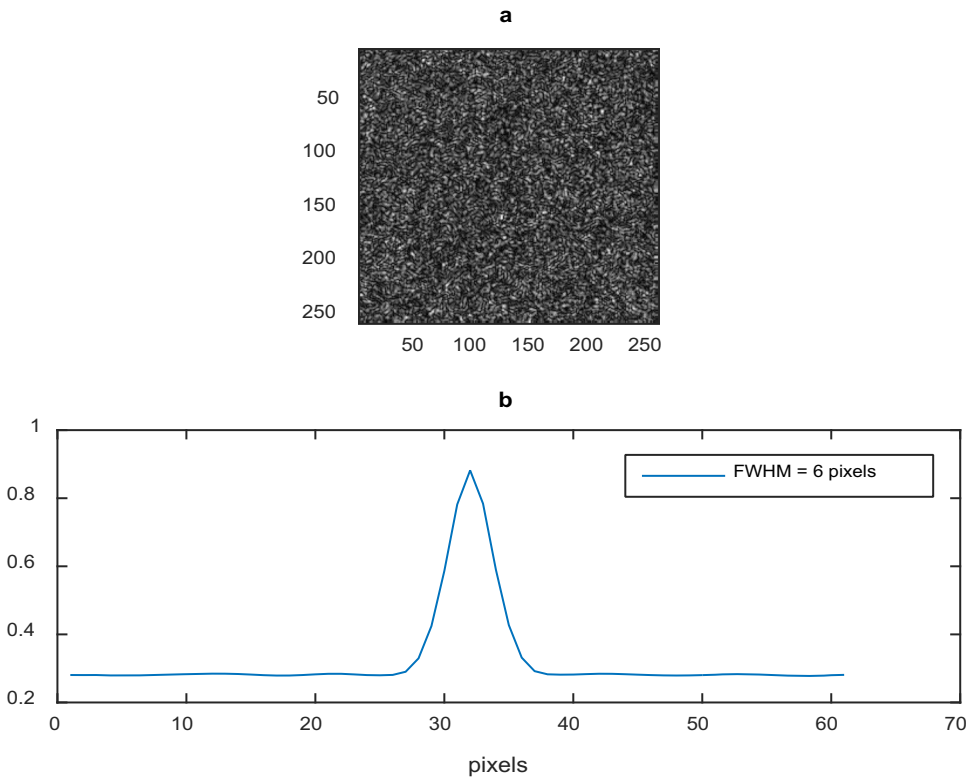

Fig. 14 **a, b** Speckle image modulated by a transparent triangular aperture (**a**), and the corresponding autocorrelation plot in (**b**) in the range from 226 to 286 pixels. The FWHM is computed as shown in the legend equal to six pixels

In addition, we showed approximately similar results for the speckle size obtained from both the PSF and the autocorrelation of speckle images corresponding to the triangular models.

Authors' contributions A single author.

Funding Open access funding provided by The Science, Technology & Innovation Funding Authority (STDF) in cooperation with The Egyptian Knowledge Bank (EKB).

Availability of data and materials Not applicable.

Declarations

Conflict of interest The authors declare that they have no competing interests.

Ethical approval Not applicable.

Consent to participate Not applicable.

Consent for publication Not applicable.

References

1. G.J. Toroldo di Francia, Resolving power and information. Opt. Soc. Am. **45**, 497 (1955)
2. C.J.R. Sheppard, A. Choudhury, Image formation in a scanning microscope. Opt. Acta **24**, 1051–1073 (1977)
3. C.J.R. Sheppard, H.J. Mattews, Imaging in high aperture optical systems. J. Opt. Soc. Am. A **4**, 1354–1360 (1987)

4. J.J. Cox, C.J.R. Sheppard, T. Wilson, Super-resolution by confocal fluorescent microscopy. Optik **60**, 391–396 (1982)
5. C.J.R. Sheppard, K.G. Larkin, Optimal concentration of electromagnetic radiation. J. Mod. Opt. **41**, 1495–1505 (1994)
6. C.J.R. Sheppard, Z.S. Hegedus, Axial behavior of pupil-plane filters. J. Opt. Soc. Am. A **5**, 643–647 (1988)
7. C.J.R. Sheppard, A. Choudhury, Annular pupils, radial polarization, and super-resolution. Appl. Opt. **43**, 4322–4327 (2004)
8. C.J.R. Sheppard, Filter performance parameters for high numerical aperture focusing. Opt. Lett. **32**, 1653–1655 (2007)
9. C.J.R. Sheppard, M. Martinez- Corral, Filter performance parameters for vectorial high aperture wave fields. Opt. Lett. **33**, 476–478 (2008)
10. A.M. Hamed, J.J. Clair, Image and super-resolution in coherent optical microscopes. Optik **64**, 277–284 (1983)
11. A.M. Hamed, J.J. Clair, Studies on optical properties of confocal scanning optical microscope using pupils with radially transmission distribution. Optik **65**, 209–218 (1983)
12. A.M. Hamed, Improvement of point spread function Optic (PSF) using linear-quadratic aperture. Optik **131**, 838–849 (2017). https://doi.org/10.1016/j.ijleo.2016.11.201
13. A.M. Hamed, T. Al-Saeed, Investigation of rectangular apertures and their application on speckle imaging. Beni-Suef Univ. J. Basic Appl. Sci. **11**, 52 (2022). https://doi.org/10.1186/s43088-022-00237-9
14. A.M. Hamed, (2021) Contrast of laser speckle images using some modulated apertures. Pramana J. Phys. **95**, 122 (2021). https://doi.org/10.1007/s12043-021-02151-8
15. A.M. Hamed, Speckle imaging of annular Hermite Gaussian laser beam. Pramana J. Phys. **95**, 202 (2021). https://doi.org/10.1007/s12043-021-02231-9)
16. T. Xu, G.R. Bashford, Resolving the lateral component of blood flow velocity based on ultrasound speckle size change with scan direction and speed, in *2009 Annual International Conference of the IEEE Engineering in Medicine and Biology Society*, Minneapolis, MN, USA, (2009), pp. 491–494.https://doi.org/10.1109/IEMBS.2009.5332618
17. S.W. Smith, R.F. Wagner, Ultrasound speckle size and lesion signal to noise ratio: Verification of theory. Ultrason. Imaging **6**(2), 174–180 (1984). https://doi.org/10.1016/0161-7346(84)90024-5